The Astrophysical Journal Letters, 829:L25 (7pp), 2016 October 1 doi:10.3847/2041-8205/829/2/L25

MAGNETAR-LIKE X-RAY BURSTS FROM A ROTATION-POWERED PULSAR, PSR J1119–6127

Ersin Göğüş[1], Lin Lin[2], Yuki Kaneko[1], Chryssa Kouveliotou[3], Anna L. Watts[4], Manoneeta Chakraborty[1], M. Ali Alpar[1], Daniela Huppenkothen[5,6], Oliver J. Roberts[7], George Younes[3], and Alexander J. van der Horst[3]
[1] Sabancı University, Orhanlı–Tuzla, İstanbul 34956, Turkey
[2] Department of Astronomy, Beijing Normal University, Beijing 100875, China
[3] Department of Physics, The George Washington University, Washington, DC 20052, USA
[4] Anton Pannekoek Institute for Astronomy, University of Amsterdam, Postbus 94249, NL-1090 GE Amsterdam, The Netherlands
[5] Center for Data Science, New York University, 726 Broadway, 7th Floor, New York, NY 10003, USA
[6] Center for Cosmology and Particle Physics, Department of Physics, New York University, 4 Washington Place, New York, NY 10003, USA
[7] School of Physics, University College Dublin, Stillorgan Road, Belfield, Dublin 4, Ireland
Received 2016 August 25; revised 2016 September 14; accepted 2016 September 14; published 2016 September 26

ABSTRACT

Two energetic hard X-ray bursts from the rotation-powered pulsar PSR J1119−6127 recently triggered the *Fermi* and *Swift* space observatories. We have performed in-depth spectral and temporal analyses of these two events. Our extensive searches in both observatories' data for lower luminosity bursts uncovered 10 additional events from the source. We report here on the timing and energetics of the 12 bursts from PSR J1119−6127 during its burst active phase on 2016 July 26 and 28. We also found a spectral softer X-ray flux enhancement in a post-burst episode, which shows evidence of cooling. Here we discuss the implications of these results on the nature of this unusual high-field radio pulsar, which firmly place it within the typical magnetar population.

Key words: pulsars: individual (PSR J1119–6127) – stars: magnetars – X-rays: bursts

1. INTRODUCTION

Episodic X-ray burst emission from magnetars has been attributed to diverse mechanisms associated with their extreme magnetic fields (∼10^{14}–10^{15} G). However, the detection of magnetar-like bursts from the young, rotation-powered pulsar (RPP) PSR J1846−0258 (Gavriil et al. 2008), and from a magnetar with a surprisingly low magnetic field, SGR 0418 +5729 (6.1×10^{12} G; similar to the typical surface dipole fields of ordinary RPPs; Rea et al. 2010; see van der Horst et al. 2010 for bursts), suggested that the two populations may actually be linked via a continuum of magnetic activity.

Typical magnetar bursts are brief (∼0.1 s long) but very luminous, reaching peak luminosities of about 10^{41} erg s^{-1} (Göğüş et al. 2001; Gavriil et al. 2004; van der Horst et al. 2012; Younes et al. 2014). These constitute the bulk of burst activity, with a few intermediate bursts of about an order of magnitude more energetic, longer durations, and long-lasting tail emission, which is much weaker than the burst but significantly above the persistent emission level (Lenters et al. 2003; Göğüş et al. 2011; Chakraborty et al. 2016).

Several mechanisms have been proposed as the source of magnetar bursts; they all assume that these are powered by their fields (for a review see Turolla et al. 2015). The crustquake model posits that the dissipation of internal magnetic energy strains the solid crust of the neutron star, which then fractures when the magnetic pressure on it becomes larger than the limiting stress it could resist. This is followed by particle acceleration and emission of radiation in the form of a short burst (Thompson & Duncan 1995). This model suggests that the bursting phenomenon maybe similar to the earthquakes, and like them, it might be governed by self-organized criticality (SOC); indeed, SOC behavior in bursting was observed in several magnetars (Göğüş et al. 1999, 2000; Gavriil et al. 2004; Scholz & Kaspi 2011), lending support to the crust-fracturing scenario. An alternative mechanism for bursts, again in the presence of extremely strong magnetic fields, is magnetic reconnection (Lyutikov 2003, 2015). In a simplified way, the scales of fracturing or reconnection (or even the combination of both processes) are reflected in the energetics of bursts (Thompson & Duncan 2001; Lyutikov 2015). Moreover, bursting activity sometimes affects radiative behavior of the source, e.g., a long-lasting increase of the persistent X-ray flux (Rea & Esposito 2011).

Contrary to magnetars, the bulk of the neutron star population is powered via the loss of their rotational energy and emit radiation as radio pulsars. RPPs have a wide range of surface magnetic fields; young objects characteristically have B-fields of about 10^{12} G. Among them, there are about 10 currently known systems with inferred surface magnetic strength in excess of 10^{13} G, with a few as high as the typical magnetar regime (Ng & Kaspi 2011). It was one of these high B-field sources (PSR J1846−0258 with $B = 4.9 \times 10^{13}$ G; Gavriil et al. 2008) that was observed emitting magnetar-like X-ray bursts. Interestingly, PSR J1846−0258 is an X-ray pulsar without observed radio emission.

PSR J1119−6127 is a young isolated neutron star among the group of high B-field systems, with a spin period of $P = 0.407$ s, and an inferred surface dipole field strength of 4.1×10^{13} G (Camilo et al. 2000). It is a highly energetic rotation-powered object ($\dot{E}$ is 2.3×10^{36} erg s^{-1}) that emits pulsed radiation spanning a wide range of the electromagnetic spectrum, including gamma-rays (Parent et al. 2011). Another intriguing property of PSR J1119−6127 is that it exhibited rotating radio transient (RRAT)-like behavior following the 2007 glitch, therefore it is the only source with glitch-induced radiative changes in radio wavelengths (Weltevrede et al. 2011; Antonopoulou et al. 2015).

The first magnetar-like triggered bursts from PSR J1119−6127 were detected with the *Fermi*/Gamma-ray Burst Monitor (GBM) on 2016 July 27 (Younes et al. 2016) and with the *Swift*/Burst Alert Telescope (BAT) on July 28 (Kennea et al. 2016). These bursts were coincident with some other extraordinary behavior. In particular, its persistent X-ray flux was increased in excess of 160-fold, and it underwent

another large glitch (Archibald et al. 2016). Additionally, its pulsed radio emission stopped following the bursts (Burgay et al. 2016a), and reappeared about two weeks later (Burgay et al. 2016b).

Here we present the results of our extensive search for additional bursts from PSR J1119−6127, and the outcomes of our detailed investigations of all identified bursts. Section 2 describes the results of our untriggered burst search in the *Fermi*/GBM and *Swift*/BAT data. In Section 3, we present the results of our detailed spectral and temporal analyses of all bursts and the persistent emission, and in Section 4 we compare the burst properties of PSR J1119−6127 with those of typical magnetar bursts, and discuss the implications of our results.

2. OBSERVATIONS

The observations described below were obtained with the *Fermi*/GBM and the *Swift*/BAT. The GBM is an all-sky monitor on board *Fermi* that is comprised 14 detectors, with an 8-sr field of view. We used GBM time-tagged event (TTE) and CTIME data, which provide data with temporal resolutions of 2 μs in 128 energy channels and 0.256 s in 8 energy channels, respectively (see Meegan 2009 for a description of the instrument and data types). The BAT is a coded aperture imager with a half-coded field of view of 1.4-sr, serving as the burst trigger instrument of *Swift* in the 15–150 keV energy range. When BAT is triggered by a burst, it records events with a temporal resolution of 100 μs in 128 energy channels (Barthelmy et al. 2005).

Fermi/GBM triggered on a burst on 2016 July 27 (trigger: bn160727543) located within the error box of PSR J1119−6127 (Younes et al. 2016). Figure 1 shows the burst light curve in three energy ranges; most of the emission is below 50 keV. Its T_{90} duration based on its photon spectrum[8] is 0.036 ± 0.009 s, and the duration obtained with a Bayesian blocks technique is $T_{\rm Bayes} = 0.040$ s. *Swift*/BAT triggered on the next day, 2016 July 28, on another burst (trigger: 706396) that was also consistent with PSR J1119−6127 (Kennea et al. 2016). The burst is soft (see Figure 2), with a Bayesian block duration estimate of 0.186 s. The event was quite faint in the GBM data (see the lower four panels of Figure 2). The T_{90} duration of this event using the GBM data is 0.240 ± 0.075 s.

We performed extensive searches in the continuous CTIME and CTTE data of *Fermi*/GBM, as well as in the readout data of the *Swift*/BAT trigger to recover bursts that were either weak or could not trigger the instruments for other reasons. We employed two independent search techniques based on a signal-to-noise ratio (S/N) and on Bayesian blocks. Both methods were optimized to search for magnetar bursts (see Kaneko et al. 2010 for the details of the S/N-based search, and Lin et al. 2013 for the Bayesian blocks search). Our searches spanned about a week, starting on 2016 July 25.

We identified five untriggered bursts from PSR J1119−6127 in the *Fermi*/GBM data, using the S/N-based search (U1, U2, U3, U5, U6 in Table 1). The burst that triggered *Swift*/BAT was also found in the GBM data but was not bright enough to pass the GBM trigger thresholds (UT2). With the Bayesian blocks algorithm, we identified 5 additional events (U4, U7, U8, U9, U10), for a total of 10 untriggered bursts. Table 1 contains[9] the list and observational details of all PSR J1119−6127 events observed with BAT and GBM.

3. SPECTRAL ANALYSIS RESULTS

3.1. Bursts

We fit the time-integrated spectrum of the GBM triggered burst (8–200 keV), starting at trigger time and covering a duration of 0.040 s, using *rmfit*.[10] The background level was determined by modeling long pre-burst and post-burst intervals. We used continuum models that best represent magnetar burst spectra: two blackbodies (BB+BB), and the Comptonized model (Compt). We also used simpler continuum models; a blackbody function (BB) and a power law (PL). We find that both BB+BB and Compt represent the spectrum well. The fit with BB+BB yields $kT_1 = 3.6 \pm 0.8$ keV and $kT_2 = 12.3 \pm 2.1$ keV (C Statistics (CStat, Cash 1979)/degrees of freedom (dof) $= 176.3/238$). Modeling with Compt results in a photon index of 1.0 ± 0.6 and a peak energy of 32.5 ± 6.4 keV (CStat/dof $= 177.8/239$). The single model fits were worse: we find for the BB temperature, $kT = 8.5 \pm 0.8$ keV (CStat/dof $= 191.6/240$) and for the PL an index $\gamma = 2.2 \pm 0.1$ (CStat/dof $= 186.8/240$). The fluence of the burst in the 8–200 keV band is $(4.1 \pm 0.4) \times 10^{-8}$ erg cm^{-2}; the corresponding luminosity and total isotropic energy are $(9.3 \pm 0.8) \times 10^{39}$ erg s^{-1} and $(3.7 \pm 0.3) \times 10^{38}$ erg, respectively, assuming a distance to the source of 8.4 kpc (Caswell et al. 2004).

The burst that triggered *Swift*/BAT was also observed in the CTTE data of *Fermi*/GBM. Therefore, we were able to perform a joint analysis of the two instrument spectra and better constrain their parameters. To this end, we extracted the BAT spectrum in the 15–150 keV band for the entire 0.18 s burst duration, and a simultaneous GBM spectrum using CTTE data in 8–200 keV. Applying the same models, we find that the BB+BB model describes the joint spectra best: $kT_1 = 3.8^{+2.2}_{-1.5}$ keV and $kT_2 = 11.0^{+1.8}_{-1.0}$ keV (χ^2/dof $= 18.1/21$). The Compt model fits the joint data but the photon index parameter could not be constrained. The fit with a single BB is also good; $kT = 9.7 \pm 0.6$ keV (χ^2/dof $= 23.3/24$), while the PL model fit is much poorer (χ^2/dof $= 35.4/24$). The fluences obtained with the BAT and GBM spectra (15–150 keV and 8–200 keV) are $(4.4 \pm 0.6) \times 10^{-8}$ and $(6.1 \pm 0.9) \times 10^{-8}$ erg cm^{-2}, respectively. The burst luminosity and total isotropic energy corresponding to the GBM fluence are $(2.8 \pm 0.4) \times 10^{39}$ erg s^{-1} and $(5.2 \pm 0.8) \times 10^{38}$ erg, respectively.

The untriggered events from PSR J1119−6127 have much lower peak intensities, while their emission lasts longer than the triggered bursts. We therefore modeled their integrated spectra uniformly with a single BB function, and obtained statistically acceptable results with a BB temperature range between 4.0 and 11.2 keV. In Table 1, we list their flux values in the 8–200 keV and 15–150 keV bands for GBM and BAT detections, respectively. Their fluences are between 7×10^{-9} and 1.1×10^{-7} erg cm^{-2}, and their corresponding isotropic energies range between 6×10^{37} and 9.3×10^{38} erg, respectively.

[8] See Lin et al. (2011a) for the description of photon spectrum based T_{90} duration measurement.

[9] An expanded version of Table 1, and the light curves of all GBM detected events are at http://magnetars.sabanciuniv.edu/psrj1119.php.

[10] http://fermi.gsfc.nasa.gov/ssc/data/analysis/rmfit/

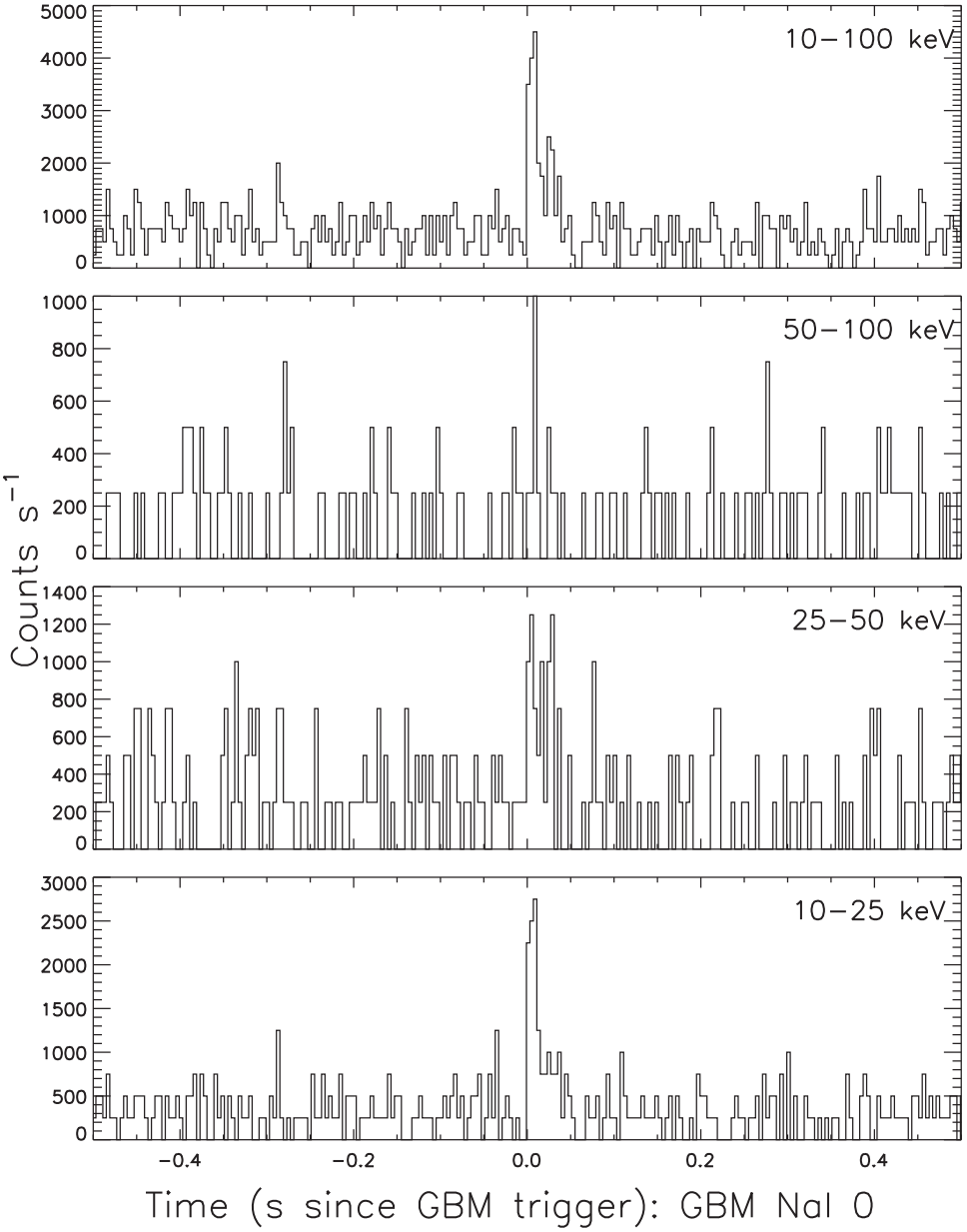

Figure 1. *Fermi*/GBM light curves of the 2016 July 27 PSR J1119−6127 burst in three energy ranges as indicated on the panels. The time resolution is 4 ms.

3.2. Enhancement of the Persistent Emission

The BAT trigger on July 28 was followed with a rapid slew toward PSR J1119−6127, and data accumulation with the *Swift*/X-Ray Telescope (XRT, Burrows et al. 2004). The XRT observations (0.5–10 keV) started ∼100 s after the BAT trigger and lasted for ∼2.2 ks in Photon Counting mode. We collected events from a circular region of radius 30″ centered on the source using the *xselect* tool, and after removing the background using a larger circular region of 141″ from a source free area, generated the light curve of the source persistent emission in 10 s time intervals. The upper panel of Figure 3 displays the XRT light curve of the source, along with the BAT observations. Two untriggered bursts in the data readout of BAT (U8 and U9 in Table 1) have also been seen in XRT. We note an X-ray flux enhancement that declined rapidly, possibly induced by the burst (see the lower panel of Figure 3).

To study the spectral evolution of the source during the flux decay, we extracted source spectra (0.5–10 keV) during time intervals corresponding to 140–810 s, 810–1580 s, and 1580–2250 s, after the BAT trigger time. We excluded the first 60 s of XRT observations to avoid contamination from bursts. We modeled all three spectra simultaneously with a BB function, which is commonly employed for the extended tails of magnetar bursts (see, e.g., Lenters et al. 2003). The fit yields a common hydrogen absorption column density of $N_{\rm H} = (1.13 \pm 0.15) \times 10^{22}$ cm^{-2} (χ^2/dof = 64.3/84). This column density is in perfect agreement with the Galactic value in the direction of the source. We found that the BB temperatures of the first two segments were consistent with each other; therefore, we linked the two temperatures and repeated the fit. We found that the BB temperature in the first two segments was 1.08 ± 0.05 keV and decayed to 0.87 ± 0.06 keV in the third (see lower panel of Figure 3). The inferred radius of the BB emitting region remains constant

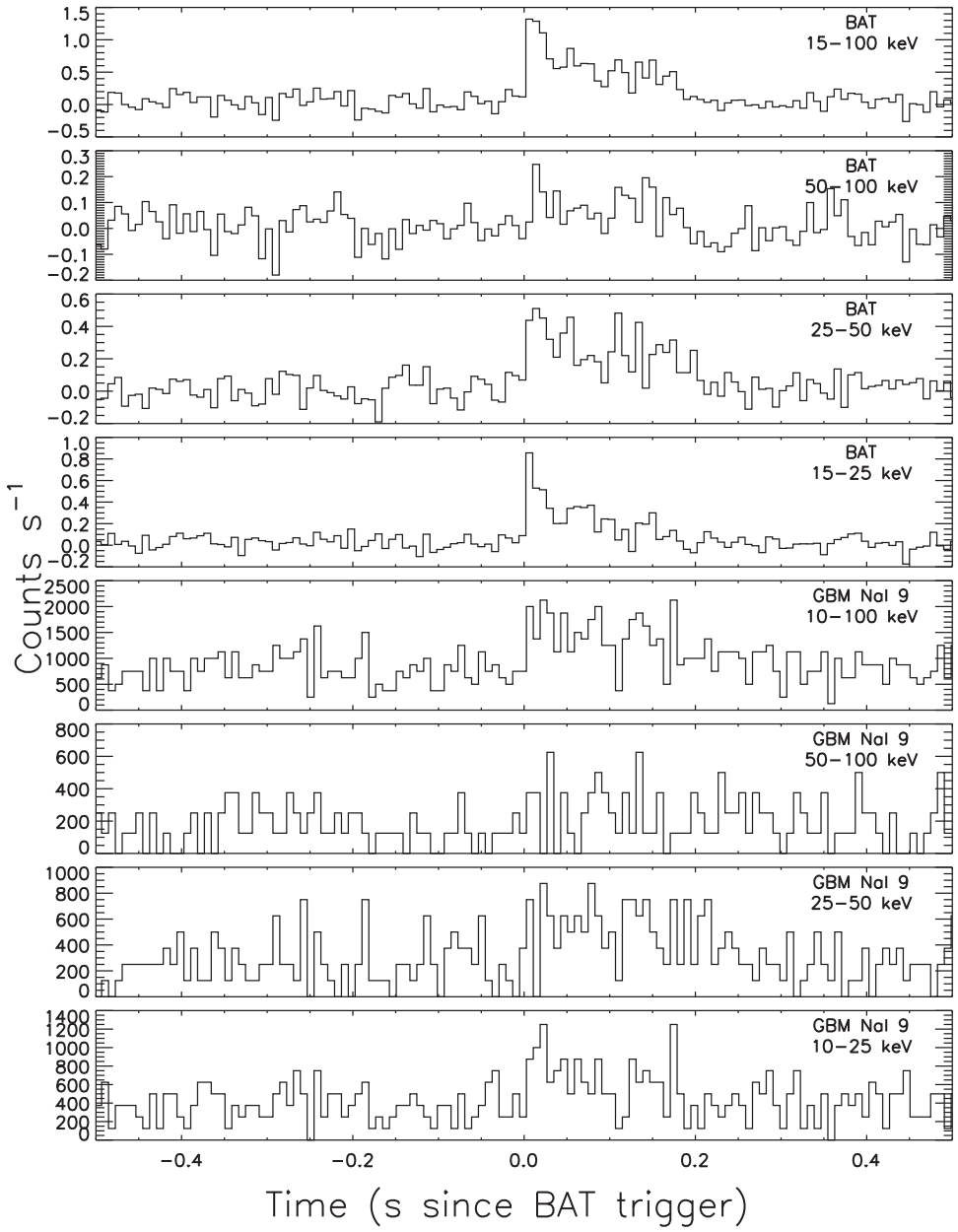

Figure 2. *Swift*/BAT light curves of the 2016 July 28 burst from PSR J1119−6127. The top four panels are obtained with the BAT data in four energy ranges (as indicated on the panels). The lower four panels are obtained with the *Fermi*/GBM data in the energy ranges indicated on the respective panels. All light curves are plotted with 8 ms time resolution.

(within errors), 1.6 ± 0.2 km. To determine the longer term temperature evolution of the persistent emission, we accumulated a spectrum from the following *Swift*/XRT pointing (Observation ID: 00034632001 with total exposure of 10 ks, spanning 57 to 92 ks after the BAT trigger). We find that the spectrum of the persistent emission modeled with a BB (and with $N_{\rm H}$ fixed at 1.13×10^{22} cm^{-2}) results in a temperature of 0.87 ± 0.01 keV, consistent with the temperature obtained during the third segment of the extended tail emission. We also modeled the spectra of the three post-burst segments simultaneously with an absorbed PL model ($N_{\rm H}$ fixed at the same value). The PL model fit is not statistically acceptable ($\chi^2/{\rm dof} = 207.2/86$); therefore, a non-thermal behavior of the enhanced X-ray emission is ruled out.

4. DISCUSSION

PSR J1119−6127 is an intriguing neutron star in many ways. The latest addition to its extraordinary properties is the emission of short but energetic hard X-ray bursts. We have performed detailed spectral and temporal investigations of the two bursts that triggered *Fermi*/GBM and *Swift*/BAT. We also performed extensive searches for lower-luminosity bursts and uncovered 10 additional events: a total of 12 bursts were detected from PSR J1119−6127 during its burst active phase of 2016 July 26–28. We obtain a cumulative energy for all 12 events as 4.8×10^{39} erg, with an average burst energy of 4×10^{38} erg. The average burst energy is around the low end of the distribution of short magnetar burst energetics, similar to the average burst energy of 1E 2259+586 (Gavriil et al. 2004).

Table 1
Swift/BAT and *Fermi*/GBM Bursts from PSR J1119−6127

Burst ID	Start Time[a] (UTC)	Instrument	Detection[b] Method	$T_{\rm Bayes}$ (s)	T_{90} (s)	Flux[c]
U1	2016 Jul 26 21:15:59.657	GBM	S/N, BB	1.456	1.8 ± 0.3	0.6 ± 0.1
U2	2016 Jul 27 12:10:42.325	GBM	S/N, BB	0.024	0.02 ± 0.02	13.8 ± 1.3
U3	2016 Jul 27 12:10:53.125	GBM	S/N, BB	0.032	0.10 ± 0.05	8.3 ± 0.8
U4	2016 Jul 27 12:19:10.294	GBM	BB	0.192	0.06 ± 0.07	1.1 ± 0.2
U5	2016 Jul 27 12:17:52.910	GBM	S/N, BB	1.000	0.8 ± 0.2	1.1 ± 1.1
T1	2016 Jul 27 13:02:07.872	GBM	S/N, BB	0.040	0.036 ± 0.009	7.8 ± 0.7
U6	2016 Jul 27 15:20:21.823	GBM	S/N, BB	0.768	0.50 ± 0.3	1.7 ± 0.2
U7	2016 Jul 27 15:45:23.156	GBM	BB	0.088	0.080 ± 0.03	3.8 ± 0.4
T2	2016 Jul 28 01:27:51.254	BAT	BB	0.180	⋯	2.4 ± 0.3
UT2[d]	2016 Jul 28 01:27:51.248	GBM	S/N, BB	0.176	0.24 ± 0.08	3.3 ± 0.5
U8	2016 Jul 28 01:29:27.234	BAT	BB	0.020	⋯	3.0 ± 1.3
U9	2016 Jul 28 01:30:02.462	BAT	BB	0.028	⋯	2.5 ± 0.5
U10	2016 Jul 28 10:47:13.690	GBM	BB	0.040	0.06 ± 0.05	4.8 ± 0.6

Notes.
[a] The start time of bursts as determined with the Bayesian blocks search.
[b] BB indicates Bayesian Blocks and S/N indicates the signal over noise ratio search method.
[c] GBM fluxes are in the 8–200 keV band; BAT fluxes are in 15–250 keV; both are in units of 10^{-7} erg cm^{-2} s^{-1}.
[d] The burst that triggered BAT.

The two triggered bursts from PSR J1119−6127, as well as all untriggered events, appear to be typical magnetar bursts.[11] Burst durations range from tens of milliseconds to about a second, similar to short bursts from other magnetars (Göğüş et al. 2001; Gavriil et al. 2004; van der Horst et al. 2012). The spectra of the two triggered bursts are well represented with the Comptonized model, or the sum of two blackbodies with temperatures of about 3 and 10 keV, in line with other magnetar bursts (Lin et al. 2011b; van der Horst et al. 2012). The duration of the burst active episode of PSR J1119−6127, and the clustering of bursts throughout this active phase resemble those of magnetars with low burst rates (Göğüş 2014). This unusual high-field radio pulsar has thus demonstrated typical magnetar behavior.

We also uncovered a probably burst-induced X-ray intensity increase that lasted about 1400 s. The enhancement is thermal in nature, with evidence of a cooling trend during the tail. Burst tails with a thermal cooling trend have been seen in other magnetars: SGR 1900+14 (Lenters et al. 2003), SGR 1806−20 (Göğüş et al. 2011), 4U 0142+61 (Gavriil et al. 2011; Chakraborty et al. 2016), and SGR J1550−5418 (Şaşmaz Muş et al. 2015). These transient enhancements were interpreted as cooling of heat imparted onto or near the neutron star surface. In the other sources, pulsed X-ray intensity was also observed to rise during the extended tail. For PSR J1119−6127, X-ray observations were performed in a mode with about 2.5 s time resolution (i.e., about 6 times the spin period of the system). Despite this, there is clearly extra heating associated with the bursts, which may come from an internal mechanism that could also give rise to the glitch (Perna & Pons 2011; Antonopoulou et al. 2015).

PSR J1119−6127 is also an exceptional radio pulsar. In 2007, after a Vela-like giant glitch ($\Delta\Omega/\Omega \sim 4 \times 10^{-6}$), some components of the radio pulse profile started to exhibit erratic RRAT-like behavior that continued for about three months (Weltevrede et al. 2011). No associated X-ray activity was reported (*Swift*, the only XRT observing the unocculted sky at the time, has a 4σ fluence sensitivity of 4×10^{-8} erg cm^{-2} in the 15–150 keV band). In its 2016 activation, PSR J1119−6127 underwent another large glitch with $\Delta\Omega/\Omega \sim 6 \times 10^{-6}$ (Archibald et al. 2016). However, the radio behavior was quite different: pulsed radio emission ceased after the bursts (Burgay et al. 2016a), reappearing two weeks later (Burgay et al. 2016b). This diversity of glitch-associated magnetospheric behavior, manifested in both radio and gamma-ray emission, is unique.

The spin recovery after the 2007 glitch was also unusual, with an over-recovery of the spin-down rate that continued to evolve on a timescale of years (Antonopoulou et al. 2015). These authors considered scenarios that could explain the unusual spin-down evolution. Superfluid mechanisms include the possibility of vortices moving inward (Akbal et al. 2015, see below), or variations in the strength of coupling between superfluid and normal components due to heating (see, e.g., Haskell & Antonopoulou 2014). Magnetospheric changes, caused by crustquakes and/or the superfluid dissipation from the glitch, were required to explain the change in radio behavior, but could in principle also explain the subsequent spin evolution.

It would, for example, fit quite naturally in the context of the model developed by Akbal et al. (2015) to account for peculiar recovery after the 2007 glitch in PSR J1119−6127. The authors suggested an extension of the standard vortex creep model (Alpar et al. 1984), the most plausible mechanism for Vela type glitches. In this model a crustquake induces both vortex unpinning (causing the glitch) and the erratic, transient, radio pulse behavior. Akbal et al. (2015) estimated the size of an individual plate involved in crust-breaking, D, in the 2007 glitch, to be about 6 m. If we assume that magnetic stresses were a dominant agent in breaking the crust and initiating the magnetar-like bursts in the 2016 outburst, and that some N pieces of crust, each of volume D^3, were involved in powering the series of 12 bursts observed, with a total energy release $E_{\rm burst} = 4.8 \times 10^{39}$ erg, $N D^3 (B^2/8\pi) = E_{\rm burst}$, we obtain the estimate $B_{14} = 2.3 \times 10^2 (D/6\,{\rm m})^{-3/2} N^{-1/2}$, where B_{14} is the

[11] The bursts from the other low field sources, PSR J1846−0258 and SGR 0418+5729, were also quite normal.

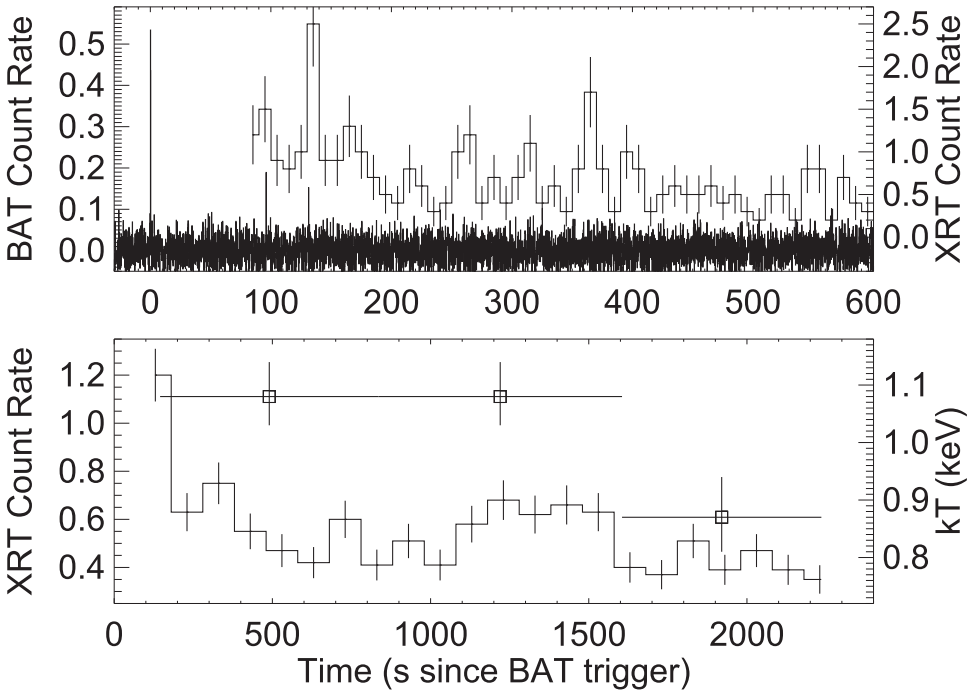

Figure 3. (Upper panel) *Swift*/BAT light curve of the PSR J1119−6127 persistent emission (15–150 keV) after the 2016 July 28 burst (left axis), with 4 ms time resolution. The right axis corresponds to the *Swift*/XRT light curve of the source (0.5–10 keV) in 10 s intervals, starting ∼100 s after the BAT trigger. (Lower panel) Extended view of the *Swift*/XRT light curve in the same energy band with 100 s bins. The squares and the right axis correspond to the BB temperatures of the persistent emission spectral fits as described in the text.

magnetic field strength in units of 10^{14} G. If we also assume that the 1.6 km radius inferred for the thermal emission covers a single surface layer of broken plates, then $N \approx (1.6\ \mathrm{km}/6\ \mathrm{m})^2$, and $B_{14} \approx 0.86$ is obtained. This means that the local surface magnetic field needed to power the bursts is larger than the inferred dipole magnetic field, but not much stronger than its strength at the pole. However, there is an uncertainty in the volume $N\ D^3$ where the magnetic energy is released. If the thermal emission radius 1.6 km is larger than the area of the surface at which the crust-breaking took place, because of the diffusion of the dissipated energy by thermal conduction or magneto-elastic waves, then N would be smaller and the estimated B_{14} could be larger.

In summary, the observations of magnetar-like bursts from PSR J1119−6127 provide the following new insights. First, they provide further evidence that global dipole fields above the quantum critical magnetic field strength are not essential for the magnetar burst trigger mechanism to operate. Since bursting has not been observed from the majority of radio pulsars it seems clear that there is some minimum field required, however, and this might motivate a detailed X-ray survey of high field radio pulsars to establish the precise threshold for bursting activity. Second, PSR J1119−6127 is the first source to demonstrate such a wide range of behavior associated with glitches and crustal heating: with variation in pulsed radio emission and now the occurrence of bursts. The superfluid, crust behavior, thermal and magnetospheric properties are an interconnected puzzle, and theoretical models must treat these elements together.

E.G. and Y.K. acknowledge support from the Scientific and Technological Research Council of Turkey (TÜBİTAK, grant No. 115F463). L.L. is supported by the Fundamental Research Funds for the Central Universities and the National Natural Science Foundation of China (grant No. 11543004). O.J.R. acknowledges support from Science Foundation Ireland under grant No. 12/IP/1288.

REFERENCES

Akbal, O., Gügercinoğlu, E., Şaşmaz Muş, S., & Alpar, M. A. 2015, MNRAS, 449, 933
Alpar, M. A., Pines, D., Anderson, P. W., & Shaham, J. 1984, ApJ, 276, 325
Antonopoulou, D., Weltevrede, P., Espinoza, C. M., et al. 2015, MNRAS, 447, 3924
Archibald, R. F., Kaspi, V. M., Tendulkar, S. P., & Scholz, P. 2016, ApJ, in press (arXiv:1608.01007)
Barthelmy, S., Barbier, L. M., Cummings, J. R., et al. 2005, SSRv, 120, 143
Burgay, M., Possenti, A., Kerr, M., et al. 2016a, ATel, 9286
Burgay, M., Possenti, A., Kerr, M., et al. 2016b, ATel, 9366
Burrows, D. N., Hill, J. E., Nousek, J. A., et al. 2004, Proc. SPIE, 5165, 201
Camilo, F., Kaspi, V. M., Lyne, A. G., et al. 2000, ApJ, 541, 367
Caswell, J. L., McClure-Griffiths, N. M., & Cheung, M. C. M. 2004, MNRAS, 352, 1405
Chakraborty, M., Göğüş, E., Şaşmaz Muş, S., & Kaneko, Y. 2016, ApJ, 819, 153
Dib, R., & Kaspi, V. M. 2014, ApJ, 784, 37
Gavriil, F. P., Dib, R., & Kaspi, V. M. 2011, ApJ, 736, 138
Gavriil, F. P., Gonzalez, M. E., Gotthelf, E. V., et al. 2008, Sci, 319, 1802
Gavriil, F. P., Kaspi, V. M., & Woods, P. M. 2004, ApJ, 607, 959
Göğüş, E. 2014, AN, 335, 296
Göğüş, E., Kouveliotou, C., Woods, P. M., et al. 2001, ApJ, 558, 228
Göğüş, E., Woods, P. M., Kouveliotou, C., et al. 1999, ApJL, 526, L93
Göğüş, E., Woods, P. M., Kouveliotou, C., et al. 2000, ApJL, 532, L121
Göğüş, E., Woods, P. M., Kouveliotou, C., et al. 2011, ApJ, 740, 55
Haskell, B., & Antonopoulou, D. 2014, MNRAS, 438, L16
Kaneko, Y., Göğüş, E., Kouveliotou, C., et al. 2010, ApJ, 710, 1335
Kennea, J. A., Lien, A. Y., Marshall, F. E., et al. 2016, ATel, 9274
Lander, S. K., Andersson, N., Antonopoulou, D., & Watts, A. L. 2015, MNRAS, 449, 2047
Lenters, G. T., Woods, P. M., Goupell, J. E., et al. 2003, ApJ, 587, 761
Lin, L., Göğüş, E., Kaneko, Y., & Kouveliotou, C. 2013, ApJ, 778, 105
Lin, L., Kouveliotou, C., Göğüş, E., et al. 2011a, ApJ, 739, 87
Lin, L., Kouveliotou, C., Göğüş, E., et al. 2011b, ApJL, 740, L16
Lyutikov, M. 2003, MNRAS, 346, 540

Lyutikov, M. 2015, MNRAS, 447, 1407
Meegan, C. 2009, ApJ, 702, 791
Ng, C.-Y., & Kaspi, V. M. 2011, in AIP Conf. Proc. 1379, Astrophysics of Neutron Stars, ed. E. Göğüş, T. Belloni, & U. Ertan (San Francisco, CA: ASP), 60
Parent, D., Kerr, M., den Hartog, P. R., et al. 2011, ApJ, 743, 170
Perna, R., & Pons, J. A. 2011, ApJL, 727, L51
Rea, N., & Esposito, P. 2011, ASSP, 21, 247
Rea, N., Esposito, P., Turolla, R., et al. 2010, Sci, 330, 944
Şaşmaz Muş, S., Aydın, B., & Göğüş, E. 2014, MNRAS, 440, 2916
Şaşmaz Muş, S., Göğüş, E., Kaneko, Y., Chakraborty, M., & Aydın, B. 2015, ApJ, 807, 42
Scholz, P., & Kaspi, V. M. 2011, ApJ, 739, 94
Thompson, C., & Duncan, R. C. 1995, MNRAS, 275, 255
Thompson, C., & Duncan, R. C. 2001, ApJ, 561, 980
Turolla, R., Zane, S., & Watts, A. L. 2015, RPPh, 78, 116901
van der Horst, A. J., Connaughton, V., Kouveliotou, C., et al. 2010, ApJL, 711, L1
van der Horst, A. J., Kouveliotou, C., Gorgone, N. M., et al. 2012, ApJ, 749, 122
Weltevrede, P., Johnston, S., & Espinoza, C. M. 2011, MNRAS, 411, 1917
Woods, P. M., Kaspi, V. M., Thompson, C., et al. 2004, ApJ, 605, 378
Younes, G., Kouveliotou, C., & Roberts, O. 2016, GCN, 19736
Younes, G., Kouveliotou, C., van der Horst, A. J., et al. 2014, ApJ, 785, 52